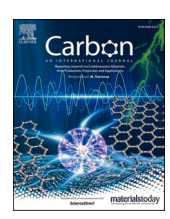


Contents lists available at ScienceDirect

Carbon

journal homepage: www.elsevier.com/locate/carbon



Check for updates

Distinct effects of endogenous hydrogen content and exogenous hydrogen supply on superlubricity of diamond-like carbon

Seokhoon Jang, Seong H. Kim

Department of Chemical Engineering and Materials Research Institute, Pennsylvania State University, University Park, PA, 16802, USA

ARTICLE INFO

Keywords: Hydrogenated diamond-like carbon Superlubricity Transfer films Graphitization Hydrogenation Run-in behavior

ABSTRACT

Hydrogenated diamond-like carbon (HDLC) has drawn significant interest as a solid lubricant coating due to its superlubricity. However, HDLC exhibits drastically different frictional behavior depending on hydrogen (H) content or sp^2/sp^3 carbon ratio. Various structural aspects of HDLC can be analyzed with Raman spectroscopy; but analyzing the wear track on the HDLC surface could not provide insightful information about the shear plane structure because the probe depth of Raman is not shallow enough to discriminate the contribution from the bulk film. When a dissimilar material is rubbed on HDLC, the transfer film is always formed on the counter-surface. Since the transfer film is the direct outcome of frictional shear, one can assume that analyzing the transfer film can depict characteristic features of the shear plane during friction without convolution from the bulk contribution. This study employed microscopic Raman analysis to capture hyperspectral images of the entire transfer films on a stainless-steel counter surface formed from HDLCs with different endogenous H-contents (30 and 40 at. % in the film) in gas environments of N_2 and H_2 (exogenous supply). This analysis provided statistically meaningful data showing how the degrees of graphitization and hydrogenation of the shear plane during the run and steady-state friction periods vary with the HDLC structure as well as the environment condition, which is critically needed information to understand how the superlubricity is induced and altered when HDLC is used as a solid lubricant film.

1. Introduction

The outstanding mechanical and tribological properties of diamondlike carbon (DLC) or amorphous carbon (a-C) have drawn great interest for various engineering applications such as protective solid lubricants on top of burls for lithographic projection apparatus [1,2] or for automobile parts [3,4]. However, its tribological performances are very different depending on its composition and structure [5] that change with synthesis conditions such as deposition temperature [6]. When DLC contains hydrogen, it is called hydrogenated DLC (HDLC). The HDLC containing about ~40 at.% hydrogen (previously known as NFC6 [7], but called 40-HDLC hereafter) is produced via a plasma-enhanced chemical vapor deposition (PECVD) process using a mixture of 25% CH₄ and 75% H₂ as a precursor gas. This 40-HDLC gives a coefficient of friction (COF; μ) as low as <0.01 in an inert environment (such as vacuum or dry N2) after a short span of run-in during which COF starts high (>0.2) and gradually decreases [8,9]. When HDLC is produced through the same PECVD method but with a precursor gas of 100% C_2H_2 , it contains ~ 30 at.% hydrogen (named as NFC10 in the original paper [7], but 30-HDLC hereafter). This 30-HDLC displays very high friction ($\mu > 0.5$) at the steady state in the same inert condition [4,10]. Moreover, these two HDLCs show a large difference in the run-in or transient periods before COF reaches the steady state [11,12]. The difference in transient friction can originate from not only H-content in the film (endogenous H) but also an external supply from environmental $\rm H_2$ gas (exogenous H). Although a large number of studies have been conducted [8,13,14], it is still puzzling why these two HDLC films with a minor difference in H-content exhibit such a drastic difference in friction.

Raman spectroscopic analysis of HDLC can provide various aspects of chemical and structural information such as the fraction of aromatic $\rm sp^2$ carbons, H-content, density, and elastic modulus based on the ratio of D-band to G-band, the full-width at half-maximum (FWHM) of G band, and fluorescent background (see Fig. S1 in the Supporting Information) [8, 15,16]. Unlike high-resolution microscopic imaging methods such as transmission electron microscopy [17,18], this spectroscopic method can provide statistically meaningful data since the probe area is relatively large. However, when this technique is employed to analyze the

E-mail address: shk10@psu.edu (S.H. Kim).

^{*} Corresponding author.

wear track in the HDLC surface formed by friction, the obtained Raman spectral features are mostly governed by the bulk film (see Fig. S2) because the typical probe depth of Raman spectroscopy is several hundred nm's, i.e., much larger than the thickness of the shear plane at the sliding interface. Such complication does not exist if the material of interest is on a substrate that does not produce any interfering signals.

In the case of HDLC friction measured with dissimilar materials such as steel or oxide balls, the formation of transfer films on the countersurface is almost always observed [8,13,19–21]. Raman analysis of the transfer film can be done without complications from the spectral contribution from the bulk substrate. Chemical information obtained by ex-situ characterizations may get convoluted due to oxidation of HDLC by exposure to air during the sample transfer since HDLC is highly susceptible to air or moisture [20,22–27]. It is noted that the surface oxidation by ambient air is a non-equilibrium process and affects only the topmost 1–2 nm region [25,26,28]. Typical thickness of transfer films is on the order of 100 nm [8]. Thus, based on the path-dependence nature of thermodynamically non-equilibrium process, one can expect the Raman analysis of the transfer film on the counter-surface to provide information on chemical and structural differences of the shear plane of the 40- and 30-HDLC films at a given frictional condition.

In this study, we investigated the correlation between the COF of HDLC and the structure of transfer films formed on a stainless steel (SS) counter-surface during the transient run-in period and after reaching the steady state using microscopic Raman analysis. Hyperspectral Raman images were obtained from the entire HDLC transfer films to assess the structural transition of transfer films. Analyzing those hyperspectral images allowed us to extract information about surface graphitization and H-content of transfer films retrieved from various stages of frictional behaviors of HDLCs tested in N_2 and H_2 environments. These analysis results allowed to construct structural models that can explain the H-content and environment dependences of the superlubricity of HDLC. This knowledge will be helpful to develop advanced solid lubricants to prevent parasitic energy loss (friction) and reduce material loss or waste (wear).

2. Experimental details

2.1. Preparation of HDLC films

Both 40- and 30-HDLC films were deposited on Si(100) wafers by the PECVD method described in the previous work [3]. In brief, the Si substrate was sputtered in an argon plasma, and then \sim 100 nm-thick silicon was deposited as a bonding layer. A reactive plasma was created from a mixture of 25% CH₄ and 75% H₂ and then the substrate was exposed to the plasma to produce \sim 1 µm-thick 40-HDLC. The same process was done with 100% C₂H₂ to produce 30-HDLC with a similar thickness. The hydrogen content of these HDLC films was previously determined with the hydrogen forward scattering (HFS) method [29].

2.2. Bidirectional ball-on-flat tribo-testing

COF was measured with a custom-made ball-on-flat bidirectional-reciprocating tribometer based on the Amontons' law [30–32]. All friction tests were repeated three to ten times to check reproducibility (Fig. S3). Before the friction test, the HDLC surfaces were rinsed with ethanol first, with deionized water next, and then blow-dried with dry nitrogen gas to remove any contaminants [33]. The HDLC sample was mounted in a continuous gas flow cell, and an AISI 440C bearing-grade SS ball with a diameter of 3 mm and a root-mean-square (RMS) surface roughness of \sim 10 nm [34] was placed on top of the HDLC substrate as the counter body with an applied load of 2 N. The reciprocating motion was conducted at a sliding speed of 3 mm/s over a span of 2.5 mm. At this sliding speed and normal load, the temperature rise produced by frictional sliding at the HDLC surfaces was estimated to be only \sim 3 K [24], which implies that the effect of frictional heat on graphitization

and hydrogenation of the shear plane is negligible in this study. The extended Hertzian contact mechanics theory [34–37] estimates the maximum contact pressure, contact radius, and deformation depth to be 1.06 GPa, 30.5 μ m, and 595 nm for 40-HDLC (elastic modulus E=55 GPa), respectively, and 1.08 GPa, 29.6 μ m, and 589 nm for 30-HDLC (E=200 GPa), respectively [5,34].

An ultrahigh purity N_2 gas (purity >99.994%; based on the supplier's specification) and a N_2 gas with 10% H_2 (premixed by supplier, purity >99.999%; hereafter called " H_2 " for simplicity) were flown continuously into the environmental cell during the friction test. All experiments were carried out at ambient pressure and room temperature. The transfer film thickness formed on the SS counter-surface after the steady-state of frictional periods was estimated to be around 110 nm from the attenuation of the SS signal in the energy-dispersive x-ray (EDX) spectroscopic imaging (Fig. S4).

2.3. Raman analyses of pristine HDLC and transfer films on SS

Raman analysis of the pristine HDLC and its transfer films was performed using a Horiba LabRam system equipped with a monochromatic 532 nm laser and a 100X objective lens with a numerical aperture of 0.9. For this setting, the probe depth of HDLC was calculated to be $\sim\!530$ nm (see Fig. S2) [38–40]. Neutral density filters were utilized to reduce the laser power to 2 mW to minimize carbon sample burning. The data acquisition time was 5 s. Since Raman analysis of random spots did not give consistent information [41], a 30 \times 30 μm^2 area of the transfer films was imaged with 15 \times 15 pixels (each pixel = 2 μm) to check the heterogeneity of the transfer film [42]. The spectral features used in the processing are graphically summarized in Fig. S1. Note that the empirical methods described here are applicable to HDLC, but not to graphite, diamond, or tertiary amorphous carbon [43]. Raman analysis at multi-wavelengths (364, 488, 532, and 634 nm) of excitation laser was done with the similar procedure.

3. Results and discussion

3.1. Structural difference between 40-HDLC and 30-HDLC

The Raman spectra of 40- and 30-HDLC are shown in Fig. 1, from which structural information of these coatings can be extracted. First, the spectral features can be deconvoluted into the D and G bands. The D band at $\sim 1350 \text{ cm}^{-1}$ originates from the breathing modes of sp² carbons in a ring structure (Fig. S1) [43,44]. The stretching modes of sp² or sp³ carbons in linear chains and ring structures produce the G band at \sim 1550 cm⁻¹ [43,44]. A higher D band and G band intensity ratio (I_D/I_G) of HDLC means a higher ratio of sp²/sp³ carbon bonds, a larger graphitic or aromatic sp²-C ring cluster, and a structurally less distorted C-C network or less deviation from a thermodynamically favorable C-C matrix or graphite [45,46]. In addition, the I_D/I_G ratio is linearly correlated with the peak position of the G band for HDLC. Thus, a higher wavenumber of the G band position is observed with more graphitic HDLC [43,44]. In Fig. 1, it can be seen that the pristine 40-HDLC have a higher I_D/I_G ratio (0.67 \pm 0.01) and a higher G band position (1552 \pm 2 $\text{cm}^{-1})$ than the pristine 30-HDLC (0.40 \pm 0.03 and 1534 \pm 4 $\text{cm}^{-1}). This$ indicates that the 40-HDLC has more graphitic structures than the 30-HDLC.

It is also noted that the 40-HDLC spectrum has a higher slope of the fluorescence background than the 30-HDLC spectrum. The ratio of the spectral background slope (m) to the peak-height intensity of the G band (I_G) is empirically shown to be proportional to the H content in HDLC (Fig. S1) [15]:

$$H[at.\%] = 21.7 + 16.6 \bullet \log\left(\frac{m}{I_G}[\mu m]\right)$$
 (1)

Using this equation, it is found that the pristine 40-HDLC and 30-

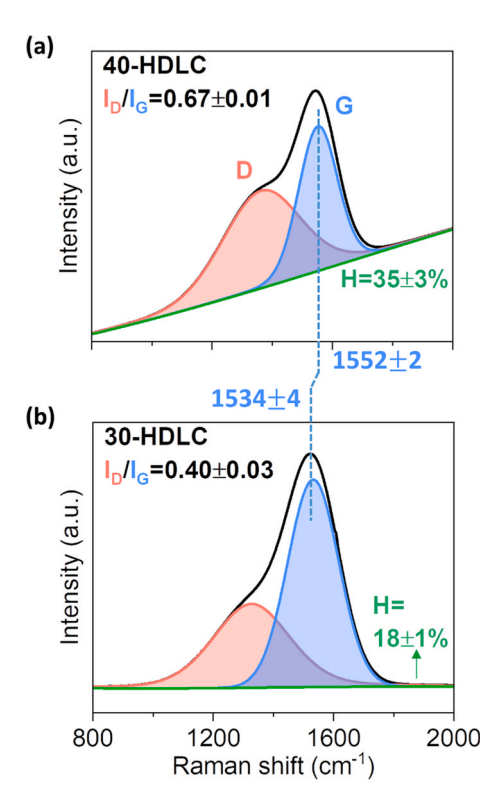


Fig. 1. Deconvoluted Raman spectra recorded from (a) pristine 40-HDLC and (b) pristine 30-HDLC surfaces. Baseline correction was not conducted for empirical estimation of endogenous H-content of HDLC. (A colour version of this figure can be viewed online.)

HDLC have \sim 35 and \sim 18 at.% of hydrogen, respectively, which is in a reasonable agreement with the H-content determined by the HFS method [29]. In addition, the density (ρ) and elastic modulus (E) of HDLC films can be empirically estimated from the FWHM of the G band (G_{FWHM}) using the following eqs [15]:

$$\rho \left[\frac{g}{cm^3} \right] = 0.257 + 0.011 \bullet G_{\text{FWHM}} \left[cm^{-1} \right]$$
 (2)

$$E[GPa] = -511 + 4.66 \bullet G_{\text{FWHM}} [cm^{-1}]$$
 (3)

From the calculation with eqs. (2) and (3), the 40-HDLC is found to have lower ρ and E than the 30-HDLC, which qualitatively match with the experimentally determined values [5,34]. The observed trend could be attributable to the more graphitic nature and higher H-content of the 40-HDLC than 30-HDLC. All structural properties of the 40- and 30-HDLC films derived from Raman analysis are summarized in Table 1. The agreement between the H-content and elastic modulus calculated from the Raman spectra and the independently-measured literature values attests that the Raman-based analysis method can provide critical structural properties of the transfer films relevant to the shear plane, although the quantitative accuracy might be limited.

3.2. Dependence of $\mu(n)$ on H-content and environment

In Fig. 2, the 40-HDLC shows a monotonic run-in behavior where COF gradually decreases to a super-lubricious value of 0.012 ± 0.003 in N_2 and a slightly higher value of 0.024 ± 0.002 in H_2 . The duration of the run-in period of 40-HDLC is found to be slightly longer in the presence of H_2 in the environment as compared to the N_2 only case. During the run-in, the initially air-oxidized surface layer of HDLC is removed [20], and transfer film is formed on the counter-surface [8,13]. The chemical and physical properties of this transfer film are known to play a critical role in the superlubricity [8,19,21].

In the case of 30-HDLC, a non-monotonic run-in behavior is observed, and the steady-state friction is significantly different in N_2 and H_2 environments. In N_2 , COF initially decreases to a minimum value (around $0.03\sim0.04$) over $5{-}10$ cycles and then increases over the next $5{-}10$ cycles to $0.85\pm0.04.$ In H_2 , the initial decrease and sudden increase in COF are similar to the N_2 environment, but the increasing trend stops at around 0.12 ± 0.06 and then COF decreases to $0.012\pm0.002.$ This non-monotonic behavior must be closely associated with the chemistry and structure of the shear plane [4,9,20,22,24,47], which could be inferred from the analysis of the corresponding transfer film.

3.3. Understanding the effect of endogenous H-content on $\mu(n)$ in inert environment

The averaged Raman spectrum and hyperspectral mapping images of the transfer film formed on SS after reaching the ultralow steady-state COF on 40-HDLC in N_2 are shown in Fig. 3. The Raman spectrum of

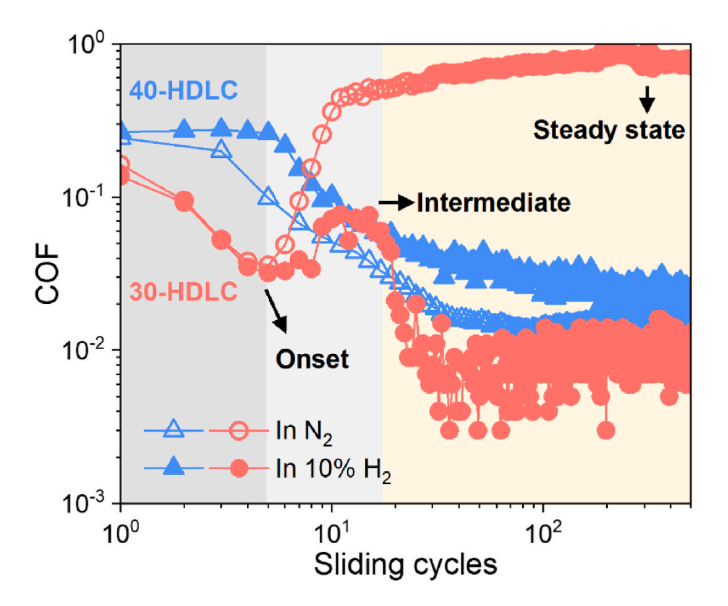


Fig. 2. Comparison of COFs measured with SS on 40-HDLC and 30-HDLC in N_2 and H_2 (76 Torr in atmospheric N_2) environments. The three different background colors correspond to the onset, the intermediate, and the steady state at 30-HDLC in H_2 to guide the eye. More data showing the reproducibility of the observed trend are shown in Fig. S3 in the Supporting Information. (A colour version of this figure can be viewed online.)

Table 1
Raman band parameters extracted from the Raman spectra of pristine 40- and 30-HDLC films and physical properties estimated using empirical correlations of Raman features. The values denoted by † and ‡ in the parentheses are from the literatures of hydrogen forward scattering (HFS) [29] and nano-indentation [5,34], respectively.

Sample	Raman band parameters			Properties calculated from Raman		
	I_{D/I_G}	G Position $[cm^{-1}]$	G_{FWHM} [cm^{-1}]	H content [at.%]	Modulus [GPa]	Density $[g/cm^3]$
40-HDLC 30-HDLC	$\begin{array}{c} 0.67 \pm 0.01 \\ 0.40 \pm 0.03 \end{array}$	$1552\pm2\\1534\pm4$	$153\pm1\\199\pm4$	$35\pm 3 \; (\sim 40^{\dagger}) \ 18\pm 1 \; (\sim 30^{\dagger})$	$egin{aligned} 200 \pm 2 \ (\sim 60^{\ddagger}) \ 415 \pm 20 \ (\sim 200^{\ddagger}) \end{aligned}$	$1.94 \pm 0.01 \\ 2.44 \pm 0.05$

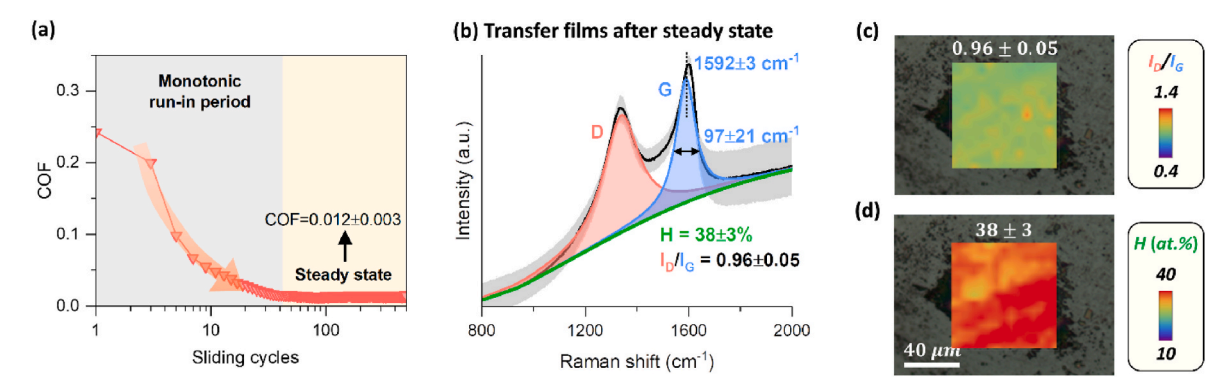


Fig. 3. (a) COF measured with SS on 40-HDLC in N_2 (excerpted from Fig. 2 and re-plotted in a linear scale of y-axis). (b) Raman spectra of the transfer films on SS retrieved after reaching the steady state COF. (c) Raman I_D/I_G maps and (d) H-content maps superimposed on the optical image of the corresponding transfer films. In (a), two different background colors are added as a guide to the eye to show the run-in period and the steady state. In (b), the grey-shaded regions indicate the standard deviation of the Raman spectrum calculated from the 225-pixel hyperspectral map. The optical image and histograms of the data in (c) and (d) are shown in Fig. S5 in the Supporting Information. (A colour version of this figure can be viewed online.)

each pixel in the hyperspectral image was processed using the same methods employed to analyze the pristine HDLC (see Section 3.1). The data indicate that the transfer film has higher I_D/I_G (0.96 \pm 0.05) and higher G-band position (1592 \pm 3 cm⁻¹) than the pristine 40-HDLC (Table 1). This means that the shear plane structure giving the superlubricity is more graphitic than the original 40-HDLC. These results suggest that shear-induced graphitization of 40-HDLC takes place at the sliding interface upon shearing in N2 to produce chemically-inert and low shear-resistant interface [4,8,10,13]. The occurrence of shear-induced graphitization on amorphous carbon or other carbon surfaces such as graphene nanocrystalline carbon has been reported in our previous study [8] and other studies [48–50]. The I_D/I_G ratio and H-content maps calculated from the hyperspectral images (Fig. 3c and d) show that the structural distribution is quite homogeneous across the entire transfer film, suggesting that shear-induced graphitization of 40-HDLC occurs relatively evenly [51,52].

The H-content of the transfer film $(38\pm3$ at.%) is almost the same or marginally increases as compared to the original film. This means that the hydrogen atoms present inside 40-HDLC are mostly conserved, or not lost, during the shear-induced graphitization. It is known that the edges of graphene exhibit significantly higher friction than the basal

plane [47,53–62]. So, if these edge sites are not properly terminated with chemically inert groups, the overall friction will be inevitably higher. Based on this fact, it can be suggested that endogenous hydrogen atoms in 40-HDLC are involved in or capable of terminating high-friction edge sites of graphitic domains formed by shear at the sliding interface, preventing the loss of super-lubricity of the graphitic shear plane.

Fig. 4 displays the averaged Raman spectra and hyperspectral mapping images of the 30-HDLC transfer films on SS retrieved right at the onset of COF rise and after reaching the steady-state COF (although fluctuating a little bit) in N₂. When the COF reaches the transfer minimum value during the run-in, the Raman features of the transfer film of 30-HDLC (Fig. 4b–i) are quite similar to those of the transfer film of 40-HDLC in the superlubricious steady state (Fig. 3b). Based on the large increase in the I_D/I_G ratio (0.92 \pm 0.06) and the G-band position (1573 \pm 7 cm⁻¹), it is obvious that the 30-HDLC film also undergoes shear-induced graphitization. Even though the pristine 30-HDLC is significantly less graphitic than the pristine 40-HDLC, the transfer film at the onset point is as graphitic as the 40-HDLC transfer film in the superlubricious state. During this initial run-in period where COF decreases to 0.04 \pm 0.01, the H-content of the shear plane (38 \pm 4%) also increases to

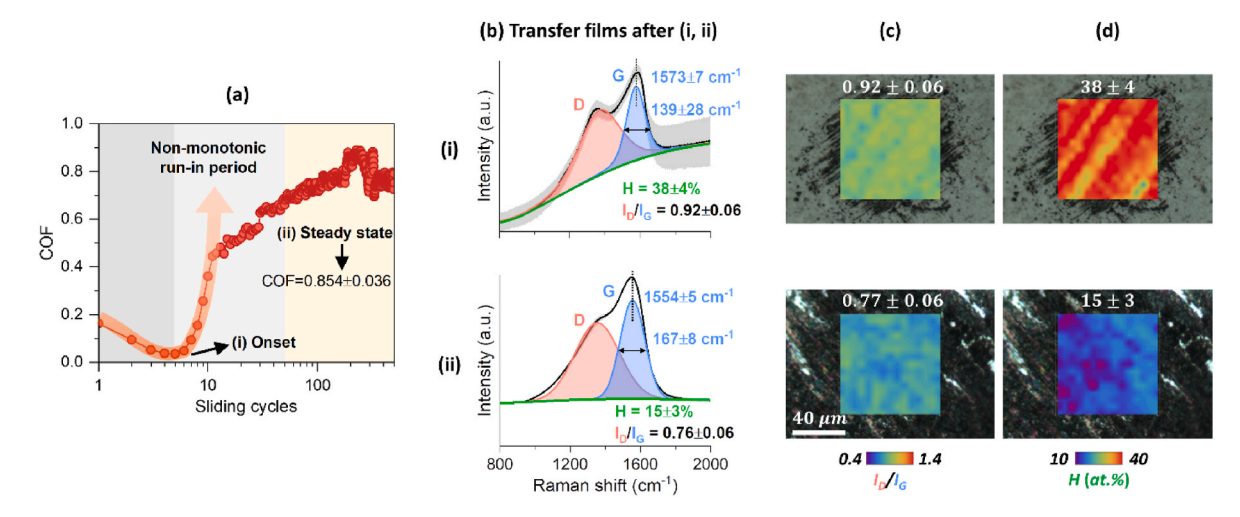


Fig. 4. (a) COF measured with SS on 30-HDLC in N_2 (excerpted from Fig. 2 and re-plotted in a linear scale of y-axis). (b) Raman spectra of the transfer films on SS retrieved after (i) the onset of the COF increase and (ii) reaching the steady state COF. (c) Raman I_D/I_G maps and (d) H-content maps superimposed on the optical image of the corresponding transfer films after the onset (upper, i) and after the steady state (lower, ii). In (a), three different background colors are added as a guide to the eye to show three regions: initial decrease, sudden increase, then gradual approach to the steady state. In (b), the grey-shaded regions indicate the standard deviation of the Raman spectrum calculated from the 225-pixel hyperspectral map. The optical image and histograms of the data in (c) and (d) are shown in Fig. S6 in the Supporting Information. (A colour version of this figure can be viewed online.)

the value comparable to the 40-HDLC transfer film in the superlubricious state ($38\pm 3\%$). The overall structure of the transfer film at the onset point appears to be relatively homogeneous (Fig. 4c-i and 4d-i).

This highly-graphitic and highly-hydrogenated state of 30-HDLC in N_2 seems unsustainable because COF increases to 0.85 $\pm~$ 0.04 immediately. The averaged Raman spectrum of the transfer film retrieved in the high friction state (Fig. 4b–ii) suggests that the shear plane structure is less graphitic ($I_D/I_G=0.76\pm0.06;$ G-band position $=1554\pm5~{\rm cm}^{-1})$ than the structure at the onset point. Moreover, the H-content of the transfer film in the high friction state (15 \pm 3 at. %) is much lower than that at the onset point. The poorly-hydrogenated transfer films can have a higher probability of forming transient covalent bonds in the sliding interface [4,11], which may result in the high COF (~20 times higher than the COF at the onset point). Similar to the onset state, the overall structure of the transfer film at the high COF state appears to be relatively homogeneous (Fig. 4c–ii and 4d-ii).

In summary, the COF measured in N_2 can be closely related to the structural parameters of the transfer films obtained from Raman analysis (see Table 2). Both 40- and 30-HDLC films undergo significant shear-induced graphitization. The major difference between these two films is that the 40-HDLC maintains the superlubricious state once it is reached, while the 30-HDLC cannot sustain the low-friction state with the high-degree of hydrogenation formed in the initial run-in. The instability of the low-friction state of the 30-HDLC must be due to the insufficient H-content in the original film; but the exact mechanism could not be deduced from this study.

3.4. Understanding the effect of exogenous H_2 supply on $\mu(n)$ of HDLC

It has been demonstrated that 30-HDLC (and other HDLCs that do not show superlubricity in vacuum or $\rm N_2$ environments) can exhibit ultralow friction in $\rm H_2$ environment [11,12,20,22,63–65]. This means that the $\rm H_2$ molecules impinging from the gas phase are involved in tribochemical reactions at the sliding interface, altering the shear plane structure in favor of achieving the superlubricity. We have studied the effect of exogenous $\rm H_2$ supply on the shear plane structure using the same Raman analysis method.

In H₂, the initial COF of the 40-HDLC film remains unchanged for a while before the run-in behavior starts (Fig. 5a and S3c), which is quite different from the run-in behavior in N₂ (Fig. 3a and S3a). It seems like that the initial air-oxidized surface layer of 40-HDLC is less susceptible to wear in H₂, although it eventually wears off. The steady-state COF is consistently higher in H₂ (0.024 \pm 0.002) compared to the N₂ case (0.012 \pm 0.003). The averaged Raman spectrum of the 40-HDLC transfer film formed in H₂ (Fig. 5b) shows that, compared to the transfer film formed in N₂, it is less graphitic ($I_D/I_G=0.87\pm0.14$; G-band position = $1584\pm13~{\rm cm}^{-1}$) and slightly more hydrogenated (42 \pm 3%). Based on the FWHM of the G-band, the transfer film formed in H₂ appears to be denser than the one formed in N₂. Also, in H₂, the transfer film structure varies locally (Fig. 5c and d). From these comparisons, it can be said that

Table 2 Relationship between COF in inert gas (N_2), Raman band parameters, and H-content of the transfer films formed from 40- and 30-HDLC surfaces after each regime in N_2 .

	40-HDLC	30-HDLC
Onset	_	0.04 ± 0.01
Steady state	0.012 ± 0.003	$\boldsymbol{0.85 \pm 0.04}$
Onset	_	$\boldsymbol{0.92 \pm 0.06}$
Steady state	0.96 ± 0.05	$\boldsymbol{0.76 \pm 0.06}$
Onset	_	1573 ± 7
		139 ± 28
Steady state	1592 ± 3	1554 ± 5
•	97 ± 21	167 ± 8
Onset	_	38 ± 4
Steady state	38 ± 3	15 ± 3
	Steady state Onset Steady state Onset Steady state Onset Steady state Onset	$ \begin{array}{cccc} \text{Onset} & - & \\ \text{Steady state} & 0.012 \pm 0.003 \\ \text{Onset} & - & \\ \text{Steady state} & 0.96 \pm 0.05 \\ \text{Onset} & - & \\ \text{Steady state} & 1592 \pm 3 \\ & 97 \pm 21 \\ \text{Onset} & - & \\ \end{array} $

the steady-state COF is quite sensitive to the degree of shear-induced graphitization and the transfer film uniformity [8,66].

Fig. 6 displays the evolution of the COF of 30-HDLC in $\rm H_2$ along with the Raman analysis result of the transfer film. At the transient minimum COF state (0.03 \pm 0.01) during the initial run-in, the Raman spectrum of the transfer film (Fig. 6b–i) shows the I_D/I_G ratio of 0.88 \pm 0.08, the G-band position at 1572 \pm 11 cm⁻¹, and the H content of 33 \pm 5 at.%, which is somewhat similar to the one formed in $\rm N_2$ (Fig. 4b–i). At the transient maximum COF state (0.12 \pm 0.06) in the intermediate run-in period, the averaged Raman spectrum (Fig. 6b–ii) is again similar to the one observed in the steady state with high COF in $\rm N_2$ (Fig. 4b–ii). As compared to the onset point, the degree of graphitization is reduced ($I_D/I_G=0.65\pm0.08$ and G-band position = 1543 \pm 5 cm⁻¹) and the degree of hydrogenation is also reduced (20 \pm 5 at.%).

After the intermediate state, the COF of 30-HDLC decreases to a superlubricious value (0.012 \pm 0.002) in H2. The averaged Raman spectrum in Fig. 6b–iii suggested that, in H2, the shear plane structure is turned back to the highly-graphitic and highly-hydrogenated state ($I_D/I_G=0.86\pm0.06$, G-band position $=1564\pm6$ cm $^{-1}$, H-content $=37\pm3$ at.%), which resembles the cases of 40-HDLC in N2 (Fig. 3b) and H2 (Fig. 5b). The overall structure of the superlubricious transfer film of 30-HDLC in H2 appears to be homogeneous (bottom panels of Fig. 6c and d), which is again similar to the 40-HDLC case in N2 (Fig. 3c and d). This implies that the exogenously supplied H2 is involved in tribochemical reactions at the sliding interface and induces the same or similar effect as the endogenous hydrogen contained in the 40-HDLC film. The structural parameters extracted from the Raman analysis of the transfer films formed in H2 are summarized in Table 3.

The data in Fig. 6 show that such tribochemical reactions involving environmental $\rm H_2$ do not occur readily on the air-oxidized 30-HDLC surface or during the initial run-in period; but they can occur readily if the degrees of share-induced graphitization and hydrogenation are reduced (i.e., at the intermediate run-in period). In fact, it has been shown that the high friction state of hydrogen-free DLC after the run-in period in Ar can be converted to the ultra-low friction state if the environment is switched to $\rm H_2$ [67]. The finding of this study suggests such transition is not just due to the increase in hydrogenation, but also associated with the increased degree of shear-induced graphitization.

Raman analysis at multi-wavelengths (364, 488, 532, and 634 nm) was conducted to estimate the $\rm sp^3$ -C content in the shear plane and the data are shown in Fig. 7. The Raman spectra collected at different excitation wavelengths can be found in Figs. S9 and S10 in the Supporting Information. The $\rm sp^3$ -carbon content of HDLC is linearly proportional to the dispersion rate of G band (Disp(G)) as following the empirical equation below [68–71]:

$$sp^{3} - C \ content = -0.07 + 2.50 \times Disp(G) \ [cm^{-1} / nm] \pm 0.06$$
 (4)

where Disp(G) is $\left|\frac{G_{Pos}^{\lambda_2}-G_{Pos}^{\lambda_1}}{\lambda_2-\lambda_1}\right|$ $[cm^{-1}/nm]$ and $G_{Pos}^{\lambda_i}$ is the position of G band at wavelength of λ_i .

The sp³-C fraction was found to be quite high (\sim 50%) for the transfer films with the high friction (μ > 0.1), i.e., 30-HDLC at the intermediate state in H₂ and steady state in N₂ (Figs. 4 and 6). All other transfer films retrieved during the low friction regime exhibited a lower fraction of sp³-carbon (\leq 25%), which indicates that the transfer films at low friction period are richer in sp²-clusters. Note that the fraction of sp¹-C (< 1%) is negligible in the diamond-like carbon [72,73]. The transfer films formed from 40-HDLC in N₂ showed the lowest sp³-carbon (\approx 5%) and the highest I_D/I_G (0.96 \pm 0.05). These results support the interpretation drawn from the I_D/I_G and position of G band in the Raman images at 532 nm (Figs. 3–6) that the extent of sp²-graphitic carbon is higher in the shear plane responsible for the ultra-low friction state.

In addition, the size of sp²-graphitic domain (L_a) is correlated with I_D/I_G as the following equation below [43]:

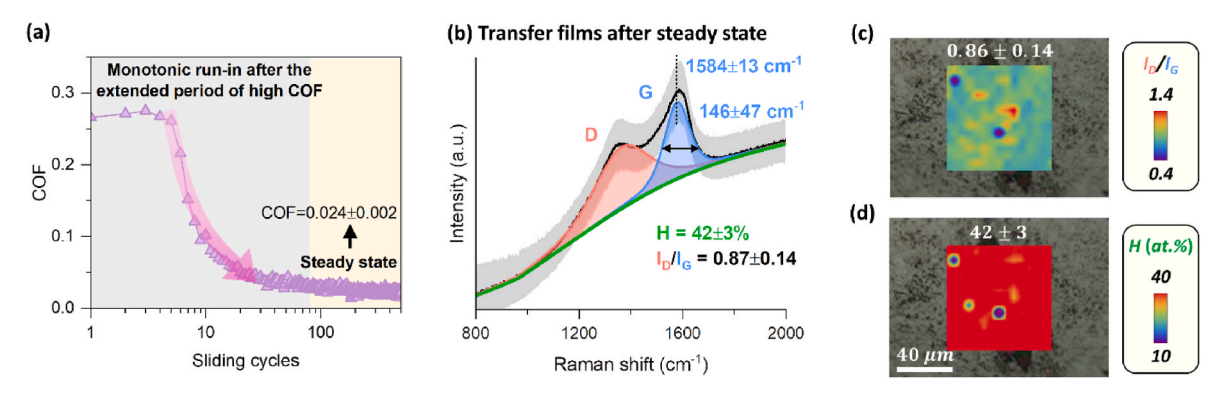


Fig. 5. (a) COF measured with SS on 40-HDLC in H_2 (excerpted from Fig. 2 and re-plotted in a linear scale of y-axis). (b) Raman spectra of the transfer films on SS retrieved after reaching the steady state COF. (c) Raman I_D/I_G maps and (d) H-content maps superimposed on the optical image of the corresponding transfer films. In (a), two different background colors are added as a guide to the eye to show the run-in period and the steady state. In (b), the grey-shaded regions indicate the standard deviation of the Raman spectrum calculated from the 225-pixel hyperspectral map. The optical image and histograms of the data in (c) and (d) are shown in Fig. S7 in the Supporting Information. (A colour version of this figure can be viewed online.)

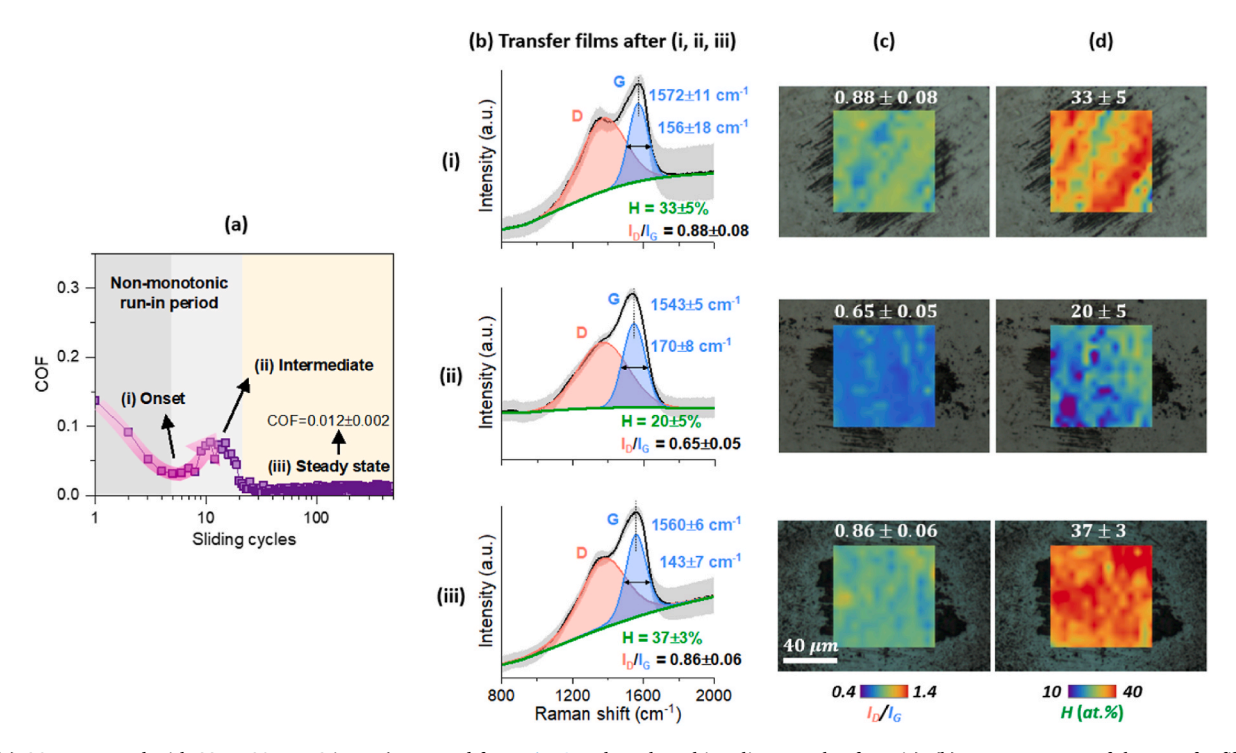


Fig. 6. (a) COF measured with SS on 30-HDLC in H_2 (excerpted from Fig. 2 and re-plotted in a linear scale of y-axis). (b) Raman spectra of the transfer films on SS retrieved after (i) the onset of the COF increase and (ii) the intermediate state, and (iii) reaching the steady state COF. (c) Raman I_D/I_G maps and (d) H-content maps superimposed on the optical image of the corresponding transfer films after the onset (upper, i), the intermediate (middle, ii), and the steady state (lower, iii). In (a), three different background colors are added as a guide to the eye to show three regions: initial decrease, sudden increase, then gradual approach to the steady state. In (b), the grey-shaded regions indicate the standard deviation of the Raman spectrum calculated from the 225-pixel hyperspectral map. The optical image and histograms of the data in (c) and (d) are shown in Fig. S8 in the Supporting Information. (A colour version of this figure can be viewed online.)

$$I_D / I_G = C'(\lambda) \bullet L_a^2 \tag{5}$$

where λ is the wavelength of Raman excitation laser and $C'(\lambda) \approx 0.0055$ at $\lambda = 514$ nm. It estimates L_a of pristine 40-HDLC and 30-HDLC to be 11 Å ($I_D/I_G = 0.67$) and 9 Å ($I_D/I_G = 0.40$), respectively. The highest I_D/I_G (0.96 \pm 0.05) observed for the transer films of 40-HDLC in N₂ corresponds to 13 Å of L_a , which also supports that the extent of sp²-graphitic domain has increased upon frictional shear.

Lastly, it is important to discuss the possible role or involvement of dangling bonds that were discussed previously [10,65,74]. The formation of dangling bonds is conceptually reasonable because every dissociation of C–C or C—C bonds will leave dangling bonds behind; but, due

to extremely high reactivity (=instability), they would be converted to other chemical species. That is one of the reasons that the DLC surface exposed by frictional shear is extremely reactive with $\rm O_2$ and $\rm H_2O$ molecules impinging from the gas phase [24]. Due to this high reactivity of dangling bonds, it is practically impossible to determine their quantity in ex-situ analysis. For that reason, the relative significance of $\rm sp^2$ -rich carbon layers (which is ascribed as graphitization) against the passivation of dangling bonds could not be determined in this study. Nonetheless, the key finding of this study is that when such oxidative reactions with environmental $\rm O_2$ and $\rm H_2O$ molecules are suppressed, then reactions with other nearby carbon atoms which are transiently brought close together and undergo graphitization by the interfacial shear process are very sensitive to the endogenous hydrogen content and

Table 3 Relationship between COF in reducing gas (H_2) , Raman band parameters, and H-content of the transfer films formed from 40- and 30-HDLC surfaces after each regime in H_2 .

		40-HDLC	30-HDLC
COF in reducing gas (H ₂)	Onset	_	0.033 ± 0.010
	Intermediate	-	0.12 ± 0.06
	Steady state	0.024 ± 0.002	0.012 ± 0.002
I_{D/I_G}	Onset	-	0.88 ± 0.08
/1 <i>G</i>	Intermediate	-	0.65 ± 0.05
	Steady state	0.87 ± 0.14	0.86 ± 0.06
Position of G $[cm^{-1}]$	Onset	-	1572 ± 11
FWHM of G $[cm^{-1}]$			156 ± 18
	Intermediate	_	1543 ± 5
			170 ± 8
	Steady state	1584 ± 13	1560 ± 6
		146 ± 47	143 ± 7
H-content [at.%]	Onset	_	33 ± 5
	Intermediate	_	20 ± 5
	Steady state	42 ± 3	37 ± 3

exogenous hydrogen supply.

4. Conclusions

This study was based on the hypothesis that the chemistry and structure of the transfer film on the counter-surface during the friction test of HDLC reflect those of shear film in action. Indeed, the hyperspectral Raman imaging of the transfer film on the SS ball surface revealed chemical and structural information that can be correlated with frictional behaviors of 40- and 30-HDLC in N2 and H2 environments. The Raman analysis results of the transfer films suggested that superlubricity of HDLC is governed by the degrees of shear-induced graphitization and hydrogenation of the shear plane, which are functions of the endogenous H-content inside the HDLC film and the exogenous H₂ supply from the environment, as graphically summarized in Fig. 8. It is important to note that the correlation of the superlubricity with the 'degree' of graphitization of the transfer film that can be identified with Raman analysis does not mean that the shear-induced structures are mostly nano-crystalline graphite domains with the longrange hexagonal order.

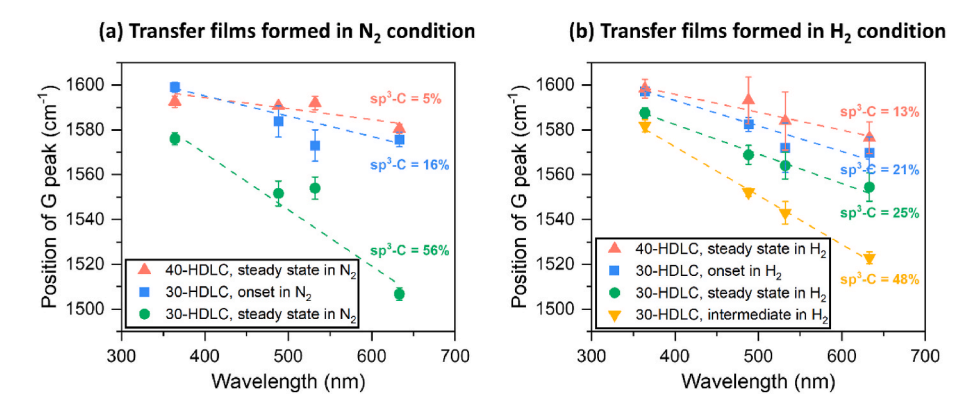


Fig. 7. Raman at multi-wavelengths (364, 488, 532, and 634 nm) for the estimation of sp^3 -C content in the transfer films formed during sliding on 30-HDLC and 40-HDLC in (a) N_2 and (b) H_2 conditions. (A colour version of this figure can be viewed online.)

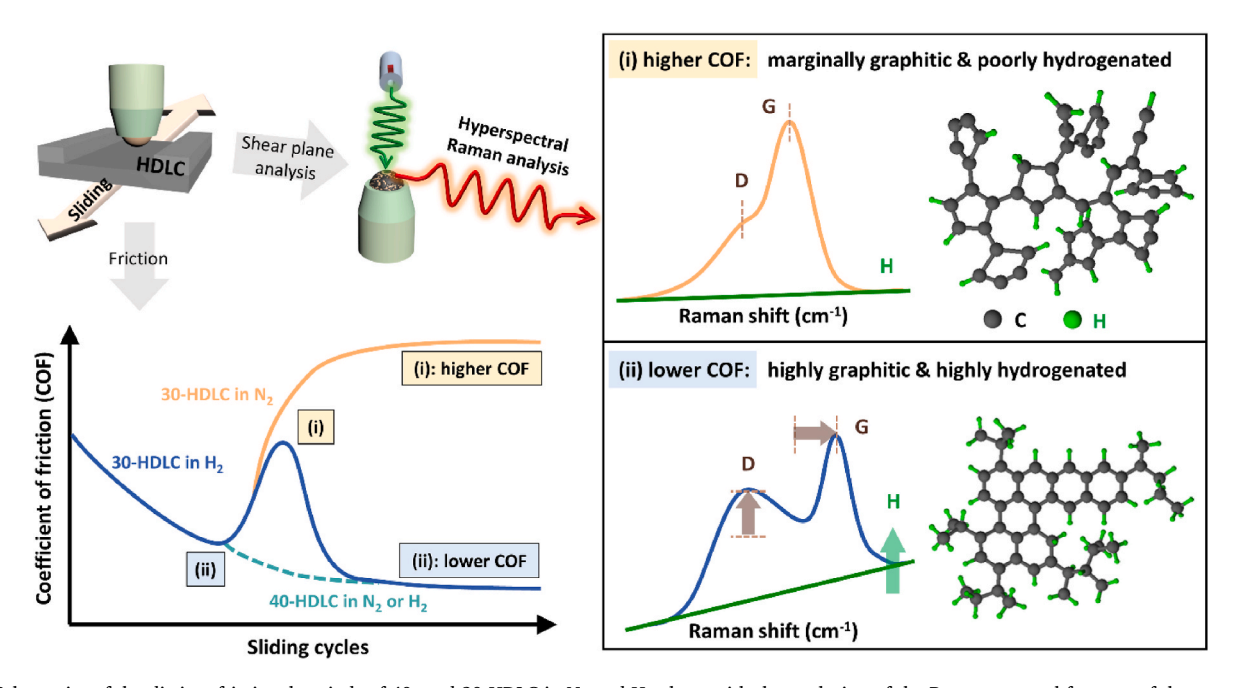


Fig. 8. Schematics of the distinct frictional periods of 40- and 30-HDLC in N₂ and H₂ along with the evolution of the Raman spectral features of the corresponding transfer films of 40- and 30-HDLC. Note that it is not drawn to scale and should be qualitatively interpreted. (A color version of this figure can be viewed online).

CRediT authorship contribution statement

Seokhoon Jang: Investigation, Data curation, Methodology, Validation, Formal analysis, Writing – original draft, Writing – review & editing. **Seong H. Kim:** Conceptualization, Investigation, Data curation, Methodology, Validation, Formal analysis, Writing – review & editing, Supervision, Project administration, Funding acquisition.

Declaration of competing interest

The authors declare that they have no known competing financial interests or personal relationships that could have appeared to influence the work reported in this paper.

Acknowledgements

This work was supported by the National Science Foundation (Grant No. CMMI-1912199). The authors acknowledge Prof. Ali Erdemir for providing HDLC samples for this study and Prof. Ashlie Martini and Prof. Brian Borovsky for discussions.

Appendix A. Supplementary data

Supplementary data to this article can be found online at https://doi.org/10.1016/j.carbon.2022.11.011.

References

- M. Lipson, D.A. Heald, I. Sigal, Lithography supports with defined burltop topography, U.S. Patent 10 (2021). June.
- [2] D. Sohrabibabaheidary, C.J. Mason, P. Helmus, M.A. Akbas, B. Albert, B. D. Dawson, Laser Roughening: Engineering the Roughness of the Burl Top, U.S. Patent, May 5, 2022.
- [3] A. Erdemir, O. Eryilmaz, I. Nilufer, G. Fenske, Synthesis of superlow-friction carbon films from highly hydrogenated methane plasmas, Surf. Coating. Technol. 133 (2000) 448–454.
- [4] A. Erdemir, C. Donnet, Tribology of diamond-like carbon films: recent progress and future prospects, J. Phys. Appl. Phys. 39 (18) (2006) R311.
- [5] Y.R. Jeng, S. Islam, K.T. Wu, A. Erdemir, O. Eryilmaz, Investigation of nanomechanical and- tribological properties of hydrogenated diamond like carbon (DLC) coatings, J. Mech. 33 (6) (2016) 769–776.
- [6] K.C. Bustillo, M.A. Petrich, J.A. Reimer, Characterization of amorphous hydrogenated carbon using solid-state nuclear magnetic resonance spectroscopy, Chem. Mater. 2 (2) (1990) 202–205.
- [7] J.A. Johnson, J.B. Woodford, D. Rajput, A.I. Kolesnikov, J.A. Schleuter, O. L. Eryilmaz, A. Erdemir, Carbon-hydrogen bonding in near-frictionless carbon, Appl. Phys. Lett. 93 (13) (2008), 131911.
- [8] P. Manimunda, A. Al-Azizi, S.H. Kim, R.R. Chromik, Shear-induced structural changes and origin of ultralow friction of hydrogenated diamond-like carbon (DLC) in dry environment, ACS Appl. Mater. Interfaces 9 (19) (2017) 16704–16714.
- [9] J. Sanchez-Lopez, A. Erdemir, C. Donnet, T. Rojas, Friction-induced structural transformations of diamondlike carbon coatings under various atmospheres, Surf. Coating. Technol. 163 (2003) 444–450.
- [10] A. Erdemir, The role of hydrogen in tribological properties of diamond-like carbon films, Surf. Coating. Technol. 146 (2001) 292–297.
- [11] J. Fontaine, C. Donnet, A. Grill, T. LeMogne, Tribochemistry between hydrogen and diamond-like carbon films, Surf. Coating, Technol. 146 (2001) 286–291.
- [12] J. Fontaine, M. Belin, T. Le Mogne, A. Grill, How to restore superlow friction of DLC: the healing effect of hydrogen gas, Tribol. Int. 37 (11–12) (2004) 869–877.
- [13] T. Scharf, I. Singer, Monitoring transfer films and friction instabilities with in situ Raman tribometry, Tribol. Lett. 14 (1) (2003) 3–8.
- [14] L. Cui, Z. Lu, L. Wang, Toward low friction in high vacuum for hydrogenated diamondlike carbon by tailoring sliding interface, ACS Appl. Mater. Interfaces 5 (13) (2013) 5889–5893.
- [15] C. Casiraghi, F. Piazza, A.C. Ferrari, D. Grambole, J. Robertson, Bonding in hydrogenated diamond-like carbon by Raman spectroscopy, Diam. Relat. Mater. 14 (3–7) (2005) 1098–1102.
- [16] L. Chen, X. Wei, G. Zhang, L. Shang, Z. Lu, X. Nie, Q. Xue, Probing the tribological performances of hydrogenated amorphous carbon film in methane atmosphere based on Hertzian elastic contact model. Tribol. Int. 155 (2021).
- [17] R.A. Bernal, P. Chen, J.D. Schall, J.A. Harrison, Y.-R. Jeng, R.W. Carpick, Influence of chemical bonding on the variability of diamond-like carbon nanoscale adhesion, Carbon 128 (2018) 267–276.
- [18] A.P. Merkle, A. Erdemir, O.L. Eryilmaz, J.A. Johnson, L.D. Marks, In situ TEM studies of tribo-induced bonding modifications in near-frictionless carbon films, Carbon 48 (3) (2010) 587–591.

[19] L. Cui, Z. Lu, L. Wang, Toward low friction in high vacuum for hydrogenated diamondlike carbon by tailoring sliding interface, ACS Appl. Mater. Interfaces 5 (13) (2013) 5889–5893.

- [20] A.A. Al-Azizi, O. Eryilmaz, A. Erdemir, S.H. Kim, Surface structure of hydrogenated diamond-like carbon: origin of run-in behavior prior to superlubricious interfacial shear, Langmuir 31 (5) (2015) 1711–1721.
- [21] Y. Liu, Y. Jiang, J. Sun, L. Wang, Y. Liu, L. Chen, B. Zhang, L. Qian, Durable superlubricity of hydrogenated diamond-like carbon film against different friction pairs depending on their interfacial interaction, Appl. Surf. Sci. 560 (2021).
- [22] M.J. Marino, E. Hsiao, Y. Chen, O.L. Eryilmaz, A. Erdemir, S.H. Kim, Understanding run-in behavior of diamond-like carbon friction and preventing diamond-like carbon wear in humid air, Langmuir 27 (20) (2011) 12702–12708.
- [23] H. Li, T. Xu, C. Wang, J. Chen, H. Zhou, H. Liu, Humidity dependence on the friction and wear behavior of diamond-like carbon film in air and nitrogen environments, Diam. Relat. Mater. 15 (10) (2006) 1585–1592.
- [24] S. Jang, Z. Chen, S.H. Kim, Environmental effects on superlubricity of hydrogenated diamond-like carbon: understanding tribochemical kinetics in O2 and H2O environments, Appl. Surf. Sci. 580 (2022).
- [25] M. Yang, M.J. Marino, V.J. Bojan, O.L. Eryilmaz, A. Erdemir, S.H. Kim, Quantification of oxygenated species on a diamond-like carbon (DLC) surface, Appl. Surf. Sci. 257 (17) (2011) 7633–7638.
- [26] N.J. Mehta, S. Roy, J.A. Johnson, J. Woodford, A. Zinovev, Z. Islam, A. Erdemir, S. Sinha, G. Fenske, B. Prorok, X-ray studies of near-frictionless carbon films, MRS Online Proc. Libr. 843 (1) (2004) 271–276.
- [27] M.A. Caro, A. Aarva, V.L. Deringer, G. Csányi, T. Laurila, Reactivity of amorphous carbon surfaces: rationalizing the role of structural motifs in functionalization using machine learning, Chem. Mater. 30 (21) (2018) 7446–7455.
- [28] F. Mangolini, J.B. McClimon, F. Rose, R.W. Carpick, Accounting for nanometer-thick adventitious carbon contamination in X-ray absorption spectra of carbon-based materials, Anal. Chem. 86 (24) (2014) 12258–12265.
- [29] J.A. Johnson, J.B. Woodford, X. Chen, J. Andersson, A. Erdemir, G.R. Fenske, Insights into "near-frictionless carbon films", J. Appl. Phys. 95 (12) (2004) 7765–7771.
- [30] V.L. Popov, Contact mechanics and friction, Springer (2010) 231–253.
- [31] X. He, Z. Liu, L.B. Ripley, V.L. Swensen, I.J. Griffin-Wiesner, B.R. Gulner, G. R. McAndrews, R.J. Wieser, B.P. Borovsky, Q.J. Wang, S.H. Kim, Empirical relationship between interfacial shear stress and contact pressure in micro- and macro-scale friction, Tribol. Int. 155 (2021).
- [32] G. Amontons, De la Resistance Cause'e dans les Machines, J. Jpn. Soc. Tribol. 44 (1999) 229–235.
- [33] A.J. Barthel, J. Luo, K.S. Hwang, J.-Y. Lee, S.H. Kim, Boundary lubrication effect of organic residue left on surface after evaporation of organic cleaning solvent, Wear 350-351 (2016) 21–26.
- [34] A. Alazizi, A. Draskovics, G. Ramirez, A. Erdemir, S.H. Kim, Tribochemistry of carbon films in oxygen and humid environments: oxidative wear and galvanic corrosion, Langmuir 32 (8) (2016) 1996–2004.
- [35] A. Fischer-Cripps, The Hertzian contact surface, J. Mater. Sci. 34 (1) (1999) 129–137.
- [36] S.B. Liu, A. Peyronnel, Q.J. Wang, L.M. Keer, An extension of the Hertz theory for three-dimensional coated bodies, Tribol. Lett. 18 (3) (2005) 303–314.
- [37] M. Kot, Contact mechanics of coating-substrate systems: monolayer and multilayer coatings, Arch. Civ. Mech. Eng. 12 (4) (2012) 464–470.
- [38] H. Harima, Raman scattering characterization on SiC, Microelectron. Eng. 83 (1) (2006) 126–129.
- [39] F. Cao, Z. He, Determination of thermal conductivity using micro-Raman spectroscopy with a three-dimensional heating model, J. Raman Spectrosc. 50 (12) (2019) 1969–1976.
- [40] D.L. Pappas, K.L. Saenger, J. Bruley, W. Krakow, J.J. Cuomo, T. Gu, R.W. Collins, Pulsed laser deposition of diamond-like carbon films, J. Appl. Phys. 71 (11) (1992) 5675–5684.
- [41] W. Gu, S. Qi, W. He, K. Chu, Z. Lu, G. Zhang, Different tribological behaviors in multilayer 2D graphene and 3D graphene foam modified DLC/H-DLC film in moist air, Tribol. Lett. 70 (1) (2022).
- [42] B.G. daFonseca, S.S. Thind, A.G. Brolo, Raman maps reveal heterogeneous hydrogenation on carbon materials, J. Raman Spectrosc. 52 (2) (2021) 516–524.
- [43] A.C. Ferrari, J. Robertson, Interpretation of Raman spectra of disordered and amorphous carbon, Phys. Rev. B 61 (20) (2000), 14095.
- [44] A. Ferrari, J. Robertson, G. Benedek, P. Milani, V. Ralchenko, Nanostructured carbon for advanced applications, J. Nano. Car. Adv. Appl. 24 (2001) 177.
- [45] X.-W. Li, M.-W. Joe, A.-Y. Wang, K.-R. Lee, Stress reduction of diamond-like carbon by Si incorporation: a molecular dynamics study, Surf. Coating. Technol. 228 (2013) S190–S193.
- [46] G. Jungnickel, T. Köhler, T. Frauenheim, M. Haase, P. Blaudeck, U. Stephan, Structure and chemical bonding in amorphous diamond, Diam. Relat. Mater. 5 (2) (1996) 175–185.
- [47] Z. Chen, A. Khajeh, A. Martini, S.H. Kim, Identifying physical and chemical contributions to friction: a comparative study of chemically inert and active graphene step edges, ACS Appl. Mater. Interfaces 12 (26) (2020) 30007–30015.
- [48] X. Chen, C. Zhang, T. Kato, X.-a. Yang, S. Wu, R. Wang, M. Nosaka, J. Luo, Evolution of tribo-induced interfacial nanostructures governing superlubricity in aC: H and aC: H: Si films, Nat. Commun. 8 (1) (2017) 1–13.
- [49] K. Sun, D. Diao, Current density effect on current-carrying friction of amorphous carbon film, Carbon 157 (2020) 113–119.
- [50] C. Chen, P. Xue, D. Diao, Graphitization vs tribo-oxidation governing friction behaviors of doped graphene nanocrystalline carbon films, Carbon 197 (2022) 435–443.

- [51] D. Bailey, R. Sayles, Effect of roughness and sliding friction on contact stresses, J. Tribol. 113 (4) (1991) 729–738.
- [52] D.T. Nguyen, P. Paolino, M. Audry, A. Chateauminois, C. Fretigny, Y. Le Chenadec, M. Portigliatti, E. Barthel, Surface pressure and shear stress fields within a frictional contact on rubber, J. Adhes. 87 (3) (2011) 235–250.
- [53] H.G. Kim, H.-B.-R. Lee, Atomic layer deposition on 2D materials, Chem. Mater. 29 (9) (2017) 3809–3826.
- [54] Z. Chen, A. Khajeh, A. Martini, S.H. Kim, Chemical and physical origins of friction on surfaces with atomic steps, Sci. Adv. 5 (8) (2019) eaaw0513.
- [55] L. Chen, Z. Chen, X. Tang, W. Yan, Z. Zhou, L. Qian, S.H. Kim, Friction at single-layer graphene step edges due to chemical and topographic interactions, Carbon 154 (2019) 67–73.
- [56] Y. Qi, J. Liu, Y. Dong, X.-Q. Feng, Q. Li, Impacts of environments on nanoscale wear behavior of graphene: edge passivation vs. substrate pinning, Carbon 139 (2018) 59–66.
- [57] M. Tripathi, F. Awaja, R.A. Bizao, S. Signetti, E. Iacob, G. Paolicelli, S. Valeri, A. Dalton, N.M. Pugno, Friction and adhesion of different structural defects of graphene, ACS Appl. Mater. Interfaces 10 (51) (2018) 44614–44623.
- [58] W. Lu, F. Qin, Y. Wang, Y. Luo, H. Wang, F. Scarpa, J. Li, R. Sesana, F. Cura, H.-X. Peng, Engineering graphene wrinkles for large enhancement of interlaminar friction enabled damping capability, ACS Appl. Mater. Interfaces 11 (33) (2019) 30278–30289.
- [59] B. Shen, Z. Ji, Q. Lin, P. Gong, N. Xuan, S. Chen, H. Liu, Z. Huang, T. Xiao, Z. Sun, Graphenization of diamond, Chem. Mater. 34 (9) (2022) 3941–3947.
- [60] Z. Chen, A. Khajeh, A. Martini, S.H. Kim, Origin of high friction at graphene step edges on graphite, ACS Appl. Mater. Interfaces 13 (1) (2021) 1895–1902.
- [61] T. Müller, M. Lohrmann, T. Kässer, O. Marti, J. Mlynek, G. Krausch, Frictional force between a sharp asperity and a surface step, Phys. Rev. Lett. 79 (25) (1997) 5066.
- [62] X. Wang, A. Dolocan, H. Chou, L. Tao, A. Dick, D. Akinwande, C.G. Willson, Direct observation of poly (methyl methacrylate) removal from a graphene surface, Chem. Mater. 29 (5) (2017) 2033–2039.
- [63] J. Andersson, R. Erck, A. Erdemir, Frictional behavior of diamondlike carbon films in vacuum and under varying water vapor pressure, Surf. Coating. Technol. 163 (2003) 535–540.

- [64] J. Andersson, R. Erck, A. Erdemir, Friction of diamond-like carbon films in different atmospheres, Wear 254 (11) (2003) 1070–1075.
- [65] Y. Qi, E. Konca, A.T. Alpas, Atmospheric effects on the adhesion and friction between non-hydrogenated diamond-like carbon (DLC) coating and aluminum—A first principles investigation, Surf. Sci. 600 (15) (2006) 2955–2965.

Carbon 202 (2023) 61-69

- [66] T.W. Scharf, I.L. Singer, Role of the transfer film on the friction and wear of metal carbide reinforced amorphous carbon coatings during run-in, Tribol. Lett. 36 (1) (2009) 43–53.
- [67] A. Erdemir, O. Eryilmaz, S. Kim, Effect of tribochemistry on lubricity of DLC films in hydrogen, Surf. Coating. Technol. 257 (2014) 241–246.
- [68] W. Cui, Q. Lai, L. Zhang, F. Wang, Quantitative measurements of sp3 content in DLC films with Raman spectroscopy, Surf. Coating. Technol. 205 (7) (2010) 1905–1909
- [69] L. Zhang, X. Wei, Y. Lin, F. Wang, A ternary phase diagram for amorphous carbon, Carbon 94 (2015) 202–213.
- [70] L. Lajaunie, C. Pardanaud, C. Martin, P. Puech, C. Hu, M. Biggs, R. Arenal, Advanced spectroscopic analyses on a: CH materials: revisiting the EELS characterization and its coupling with multi-wavelength Raman spectroscopy, Carbon 112 (2017) 149–161.
- [71] A. Merlen, J. Buijnsters, C. Pardanaud, A guide to and review of the use of multiwavelength Raman spectroscopy for characterizing defective aromatic carbon solids: from graphene to amorphous carbons, Coatings 7 (10) (2017).
- [72] M.D.B. Bouchet, C. Matta, T. Le-Mogne, J.M. Martin, Q. Zhang, W. Goddard III, M. Kano, Y. Mabuchi, J. Ye, Superlubricity mechanism of diamond-like carbon with glycerol. Coupling of experimental and simulation studies, in: Journal of Physics: Conference Series, IOP Publishing, 2007, 012003.
- [73] S. Neuville, A. Matthews, A perspective on the optimisation of hard carbon and related coatings for engineering applications, Thin Solid Films 515 (17) (2007) 6619–6653
- [74] O. Eryilmaz, A. Erdemir, TOF-SIMS and XPS characterization of diamond-like carbon films after tests in inert and oxidizing environments, Wear 265 (1–2) (2008) 244–254.